ChemComm

Accepted Manuscript

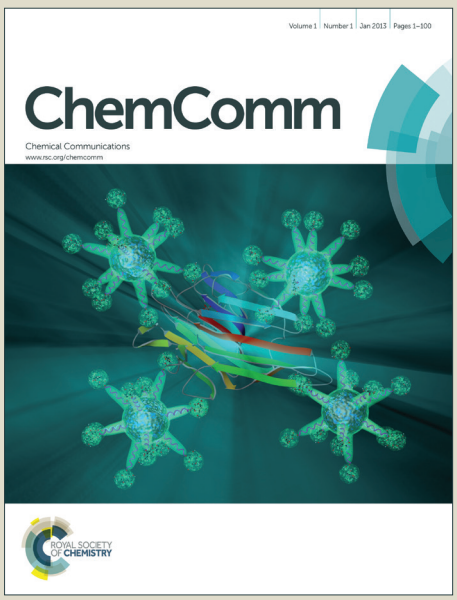

ROYAL SOCIETY OF CHEMISTRY

www.rsc.org/chemcomm

ChemComm

COMMUNICATION

A facile Pt catalyst regeneration process significantly improves the catalytic activity of Pt-organic composites for the O_2 reduction reaction

Received 00th January 20xx,
Accepted 00th January 20xx

DOI: 10.1039/x0xx00000x

www.rsc.org/

Jing-Fang Huang* and Wen-Yu Chen

Combination of the "nano-size" effect and Cl^- complexation ability causes massive electrodissolution of Pt under acidic conditions to promote the regeneration of Pt-organic composites and to significantly improve the catalytic performance of the O_2 reduction reaction.

Despite significant recent advances, poor durability of the Pt catalyst for the oxygen reduction reaction (ORR) in fuel cell cathodes and its high content in catalysts remain the key challenges that hinder the widespread commercialization of this technology.[1-4] The proton exchange membrane fuel cell (PEMFC) is a highly efficient power-generation system incorporating a poly(perfluoroalkylsulfonic acid) such as Nafion (NF) as the electrolyte membrane and proton conductor. In the PEMFC, a Pt-based electrocatalyst, believed to be a noncorrosive material, is generally used for the cathode.[1, 2, 5] However, the long-term operation of PEMFCs causes loss of the Pt electrochemical surface area (ECSA) over time because of corrosion of the carbon support and Pt dissolution/aggregation/Oswald ripening, which is considered one of the major contributors to the degradation of fuel cell performance.[6, 7] Extensive research has focused on the reduction of Pt size and content to higher performance and to lower the cost of fuel cell materials but also on the development of alternative non-carbon support materials such as metals, nitrides, conducting polymers, and metal oxides for fuel cell catalysts to improve the durability of catalysts.[2, 3, 8] To address the sustainability of catalytic materials, it is necessary to consider either recycling or regenerating Pt and other precious metal catalysts or catalytic materials.[9-11] This is a challenging task, whose first step requires a facile process for the massive dissolution of Pt. In our previous studies, massive electrodissolution of bulk Pt was realized in basic 25–75 mol% zinc chloride-1-ethyl-3-methylimidazolium chloride ($ZnCl_2$-EMIC) ionic liquid; however, Pt is still considered one of the "noblest" noble metals in aqueous solution.[9] The stability of Pt decreases with particle size, especially for sub-5 nm particles, resulting in the gradual dissolution of Pt nanoparticles (nPts) during the operation of a fuel cell.[12] Here, we develop a facile approach to significantly accelerate the massive dissolution of nPts by using anodic cyclic voltammetry in a dilute aqueous solution of HCl (0.5 M) containing 0.5 M $NaClO_4$. We also applied this process to address, for the first time, the regeneration of a new non-carbon supported nPt catalyst for the ORR. In our previous study, an EC′ catalytic process, Cu^+-mediated Pt reduction (CMPR), was successfully used to incorporate monodisperse nPts in the NF as a non-carbon support (Scheme 1 and ESI†).[13, 14] During multiple-scan cyclic voltammetry (MSCV), monodisperse nPts repeatedly formed in the NF and an nPt-embedded NF (NF(Pt_{nano})) composite was fabricated by this process.[13] The NF(Pt_{nano}) composite was demonstrated as a potential non-carbon-supported nPt catalyst for the ORR. In this study, this NF(Pt_{nano}) composite was selected to prove the regenerability of the ORR catalyst, because its Pt content is readily controllable. Surprisingly, it was possible to successfully regenerate the catalyst; the study also showed an unexpectedly noteworthy enhancement in the catalytic performance of the ORR.

Typically, HCl-dependent cyclic voltammograms (CVs) of bulk Pt and NF(Pt_{nano})-modified glassy carbon electrode (NF(Pt_{nano})@GCE) are recorded in 0.5 M $NaClO_4$ aqueous solutions

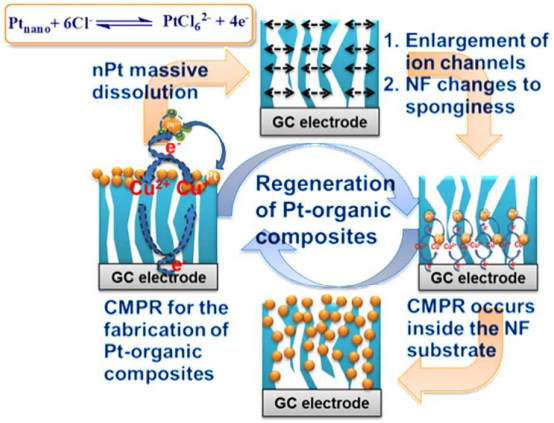

Scheme 1 A mechanism of regeneration of NF(Pt_{nano}) composite

Department of Chemistry, National Chung Hsing University, Taichung, 402, Taiwan, R.O.C. E-mail: jfh@dragon.nchu.edu.tw

Electronic Supplementary Information (ESI) available: [Experimental procedures: fabrication of NF(Pt_{nano}) composites, electrodissolution of nPts, and electrochemical characterization of ORR.]. See DOI: 10.1039/x0xx00000x

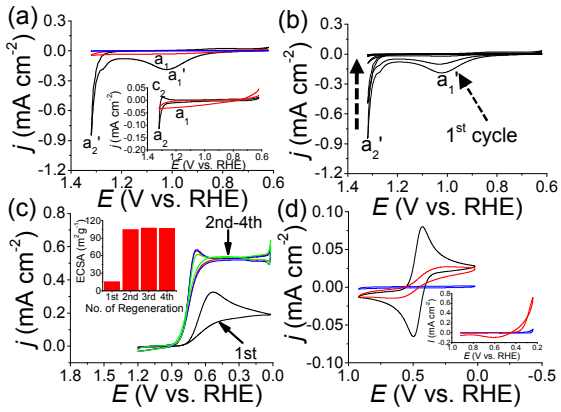

Fig. 1 (a) CVs of bulk Pt (inset), NF(Pt_{nano})@GCE and GC (blue line) were recorded in 0.5 M $NaClO_4$ aqueous solutions with (black line) and without (red line) 0.5 M HCl, respectively; (b) The MSCV of the NF(Pt_{nano})@GCE in 0.5 M $NaClO_4$ solution containing 0.5 M HCl was recorded at a scan rate 0.01 V s^{-1}. (c) CVs for ORR at each regenerated NF(Pt_{nano})@GCEs (from the 1st to the 4th generation) recorded in an O_2-saturated 0.1 M $HClO_4$ aqueous solution at a scan rate 0.01 V·s^{-1}. The inset is the specific ECSA (ECSA/Pt loading, $m^2 \cdot g^{-1}$) for each regenerated NF(Pt_{nano})@GCEs. (d) CVs of $Fe(CN)_6^{3-/4-}$ were recorded on NF(Pt_{nano}/dePt_{nano})@GC (red line), NF@GC (blue line), and GC (black line) electrodes at a scan rate of 0.05 V·s^{-1}. Inset shows the first cycle of CVs in CMPR recorded on NF(Pt_{nano}/dePt_{nano})@GC(red line) and NF@GC (blue line) electrodes, respectively.

(Fig. 1a). In the absence of HCl, an anodic wave a_1, corresponding to the formation of platinum oxide (PtO_x) on the surface of the electrode, is observed for both bulk Pt and NF(Pt_{nano})@GCE in the anodic potential sweeping.[15] After adding 0.5 M HCl, the anodic wave a_1 on the bulk Pt is replaced by a sharply increased anodic current at 1.25 V vs. RHE (anodic wave a_2); an accompanying cathodic wave c_2 is also observed on the reverse scan (inset of Fig. 1a). The wave couple, a_2/c_2, at the anodic potential limit is assigned to the redox process between Cl^- and Cl_2, because the redox currents are a function of the HCl concentration (Fig. S1a, ESI†). The disappearance of anodic wave a_1 also implies that the adsorption of the $PtCl_x^{(x-2)-}$ complex, i.e., either $PtCl_2$ or $PtCl_4^{2-}$, occurs on the Pt substrate to hinder the formation of PtO_x and their continuous anodic dissolution from the Pt surface.[11] Surprisingly, in the same HCl-containing electrolyte solutions, we observed an exceptional anodic stripping peak a_1' and a significant increase in the anodic current at the anodic potential limit (anodic wave a_2') on the NF(Pt_{nano})@GCE. Thus, new anodic reactions on the NF(Pt_{nano})@GCE can be induced with the introduction of 0.5 M HCl. To determine HCl-induced reactions, the MSCV of the NF(Pt_{nano})@GCE was recorded in a 0.5 M $NaClO_4$ solution containing 0.5 M HCl in the same potential region at a scan rate of 0.01 V·s^{-1}, whereupon the anodic waves a_1' and a_2' rapidly diminished to the background signal of the NF-coated glassy carbon electrode (NF@GC) by the third potential sweeping cycle (Fig. 1b). This implies that nPts in the NF(Pt_{nano})@GCE are anodically stripped during the anodic potential sweeping. The signature voltammetric features of Pt, i.e., the formation and reduction of PtO_x (0.4–1.2 V vs. RHE) and the adsorption or desorption of hydrogen (0.3–0.0 V vs. RHE), on the NF(Pt_{nano})@GCE in 0.5 M H_2SO_4 also disappear and only leave a clear NF@GC background response after the anodic MSCV treatment (Fig. S1b, ESI†). This strongly suggests that anodic waves a_1' and a_2' are induced by Pt anodic dissolution; however, the same phenomenon is not observed for bulk Pt. nPts (especially for the sub-5 nm scale particle size) have a higher solubility than bulk Pt.[12] In an acidic environment, Pt solubility increases as the pH decreases. Although Pt can dissolve in non-complexing acids (such as H_2SO_4 and $HClO_4$) under anodic conditions (potential cycling, constant potential, or constant current), these studies showed that the Pt dissolution rate was still very low. In this regard, potentiostatic dissolution rates of 1.4×10^{-8} and 1.7×10^{-8} μg·cm^{-2} s^{-1} were reported at 0.9 V for a 10 wt% Pt/C catalyst and Pt wire, respectively, in $HClO_4$ solution.[16] In this study, the Pt dissolution rate increased significantly to 0.42 μg·cm^{-2} s^{-1} in the presence of 0.5 M HCl. This result is not only attributed to the "nano-size" effect and acidic conditions, but also to the complexing ability of the Cl^- ion. Further identification of the dissolved Pt ions was conducted by evaluating the anodic charge used for anodically stripping nPts from NF(Pt_{nano})@GCEs with a known mass of Pt during the anodic MSCV treatment. The related data are shown in Fig. S2a and Table S1 (ESI†). In accordance with Faraday's laws of electrolysis, the results of these experiments confirmed that Pt^{4+} is the major product of the anodic MSCV treatment.[15] In Fig. S2b (ESI†), CVs dependent on the Pt^{2+} content were recorded in a 0.5 M $NaClO_4$ solution containing 0.5 M HCl. The use of various concentrations of $PtCl_4^{2-}$ showed that the oxidation of Pt^{2+} occurred at a potential close to that of anodic wave a_2' without any response in the potential range of wave a_1'. It demonstrates that the production of Pt^{4+} predominantly occurs at oxidation wave a_2'. These results show that Pt is oxidized to Pt^{2+} at oxidation wave a_1' and to Pt^{4+} at oxidation wave a_2' on the anodic potential sweep. The broadness of oxidation wave a_1' is also consistent with the formation of surface-bound Pt chloride complexes such as $PtCl_2$ or $PtCl_4^{2-}$.[17] The formation of a soluble Pt^{4+} complex such as $PtCl_6^{2-}$ could occur at wave a_2'.[7] The NF(Pt_{nano}) composite capable of facilitating the ORR has been demonstrated in previous studies, which showed that the catalytic performance could be considerably enhanced by increasing the Pt load of the NF(Pt_{nano}) composite to above 40 μg·cm^{-2}.[13] Reduction of the Pt load and realizing the regeneration of catalysts are significant challenges in the development of electrocatalysts. The regenerability of the NF(Pt_{nano}) composites was confirmed by the anodic stripping of nPts from the NF(Pt_{nano}) composites after ORR tests and re-embedded by CMPR. Fig. 1c shows the CVs for the ORR at each regenerated NF(Pt_{nano})@GCE recorded in an O_2-saturated 0.1 M $HClO_4$ aqueous solution. The NF(Pt_{nano})@GCE with ultra-low Pt loading (5 μg cm^{-2}) is selected as a model system for this discussion. A well-defined reduction peak is observed on the first generation of NF(Pt_{nano})@GCE (NF^{1st}(Pt_{nano})@GCE) at ~0.58 V (vs. RHE) and the catalytic current density was ~0.32 mA·cm^{-2} at a scan rate of 0.01 V·s^{-1}. Surprisingly, the reduction peak potential on the second generation of NF(Pt_{nano})@GCE (NF^{2nd}(Pt_{nano})@GCE), which is the re-embedding of nPts into the initially regenerated NF-coated GC electrode (NF^{1st}@GCE) from the NF^{1st}(Pt_{nano})@GCE after anodic stripping of the nPts occurs at ~0.75 V (vs. RHE), is 170 mV more positive than on the NF^{1st}(Pt_{nano})@GCE. Moreover, the catalytic current density (~0.6 mA·cm^{-2}) was 1.88 times greater than that of

the $NF^{1st}(Pt_{nano})$@GCE. The regenerability of $NF(Pt_{nano})$ composites is strongly suggested by the fact that similar catalytic performances were observed in each different generation of $NF(Pt_{nano})$@GCEs except for the $NF^{1st}(Pt_{nano})$@GCE. A significant improvement in the catalytic performance was also observed for each regenerated $NF(Pt_{nano})$@GCEs. The ECSA is one of the most important properties of electrocatalysts. The CVs of the initial and regenerated $NF(Pt_{nano})$@GCEs recorded in 0.2 M H_2SO_4 from 1.2 to 0.0 V (vs. RHE) at 0.2 $V{\cdot}s^{-1}$ are shown in Fig. S3 (ESI†). The ECSA was calculated from the charge under the voltammetric peaks for hydrogen adsorption or desorption (0.3–0.0 V vs. RHE) using the reported value of 0.21 $mC{\cdot}cm^{-2}$ for a clean Pt surface.[15] A significant increase in the ECSA was also observed for the regenerated $NF(Pt_{nano})$@GCEs (Fig. S3, ESI†). The specific ECSA (ECSA/Pt loading, $m^2{\cdot}g^{-1}$) was greatly increased to 108–112 $m^2{\cdot}g^{-1}$ after regeneration, an area that is much larger than that of the initial $NF^{1st}(Pt_{nano})$@GCE (~25 $m^2{\cdot}g^{-1}$) (Fig. 1c inset). This also provides direct evidence for the improvement in the catalytic performance of the regenerated $NF(Pt_{nano})$@GCEs. A possible reason for this remarkable improvement could be the micro-morphological change of the regenerated NF substrate that could further affect the process of Pt reduction and the distribution of nPts. CVs of the anionic redox probe, $Fe(CN)_6^{3-/4-}$, were used to understand the variation of NF in the regeneration of $NF(Pt_{nano})$ composites (Fig. 1d). Fig. 1d shows the redox signal of $Fe(CN)_6^{3-/4-}$ to be completely inhibited on NF@GCE because of the fluorocarbon backbone and the negative Donnan effect from $-SO_3^-$ in the NF.[18] The redox response of $Fe(CN)_6^{3-/4-}$ is regenerated on the NF@GCE, which was treated by embedding the nPts in and subsequently stripping of (NF(Pt/dePt)@GCE), although the current intensity is still lower than that on bare GCE. This result indicates that, after the treatment of Pt/dePt, the anionic permeability of NF increases, thereby greatly reducing the overpotential of the CMPR owing to the source of anionic Pt complexes ($PtCl_4^{2-}$) capable of reacting with mediator Cu^+ inside the NF membrane and further reducing the mass transfer resistance of the Cu^+ mediator in the NF (Fig. 1d inset).

Fig. 2a–d show the representative scanning electron microscopy (SEM) and transmission electron microscopy (TEM) images, respectively, of the $NF^{1st}(Pt_{nano})$ and $NF^{2nd}(Pt_{nano})$ composites. The SEM images of the bare NF (Fig. S4a,b, ESI†) resemble the description of the cluster-network model of NF composed of spherical clusters with diameters of approximately 4–5 nm, interconnected by hypothetical channels of approximately 1 nm.[18] The SEM images of the $NF^{1st}(Pt_{nano})$ composite show enlarged channels and a number of spherical light spots (nPts) with diameters of approximately 2–5 nm dispersed along the edges of the channels and spherical holes (clusters) (Fig. 2a and S4d, ESI†). In the lower-magnification images (Fig. 2a inset and Fig. S4c, ESI†), many larger Pt spherical particles with a diameter of approximately 200 nm are found on the NF surface besides the ultra-small nPts (2–5 nm) located on the clusters. A vast increase in the porosity of the structures is observed in the SEM images of the $NF^{2nd}(Pt_{nano})$ composite (Fig. 2c and S4f, ESI†), indicating that Pt/dePt renders the microstructure of the NF substrate highly porous and spongy. This could be due to an enlargement in the size of the ion channels after the Pt/dePt process. Interestingly, only well-dispersed and highly dense ultra-small nPts (2–5 nm) were found on the edge of the

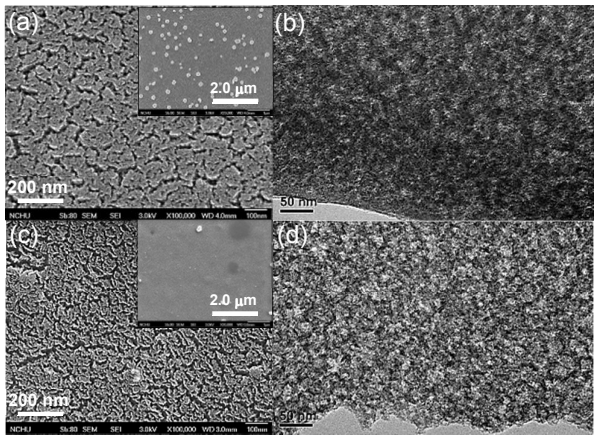

Fig. 2 SEM images of (a) $NF^{1st}(Pt_{nano})$ and (c) $NF^{2nd}(Pt_{nano})$ composites. Insets show SEM images of (a) and (c) taken at lower magnification. TEM images of (b) $NF^{1st}(Pt_{nano})$ and (d) $NF^{2nd}(Pt_{nano})$ composites.

porous channels and spherical clusters in the absence of larger Pt spherical particles (Fig. 2c inset and Fig. S4e, ESI†). This may owing to the larger surface area provided by the sponge-like regenerated NF substrate, which provides more space for the dispersion of nPts. The TEM image of the $NF^{1st}(Pt_{nano})$ composite shows well-dispersed, highly dense nPts (dark spots) with nearly spherical shapes and a narrow size distribution of 2–5 nm (Fig. 2b and S5a,b, ESI†). This result is consistent with the SEM images. In addition to the dark spots, there were light and gray regions. The image exhibits a dense texture of spherical light areas (porous structure) of approximately 5-10 nm in diameter and homogeneously distributed in the NF film. The gray and light areas correspond to the fluorocarbon backbone and ionic clusters in the NF, respectively.[19] On the TEM image of the $NF^{2nd}(Pt_{nano})$ composite (Fig. 2d and S5c,d, ESI†), the light areas are greatly enlarged and expanded and a large number of spherical dark spots (nPts) with a narrow size distribution of 2–5 nm are clearly identified owing to the improved dispersion of the nPts on the $NF^{1st}(Pt_{nano})$ composite. The analyses of these images suggest that the Pt/dePt process transforms the micro-morphology of NF to become highly porous and spongy, thereby enhancing its suitability as a catalyst substrate. The formation of a highly porous microstructure and the enlargement of the ion channels also illustrate the increasing ionic permeability in the regenerated NF substrate that significantly reduces the mass transfer resistance of the Cu^+ mediator and O_2 reactant in the CMPR and the ORR, respectively. As indicated by the mechanism proposed in Scheme 1, we believe the highly porous surface area found on the regenerated NF substrate enables the CMPR process to fully utilize the interior of the ion channel and NF substrate.

Fig. 3 shows the typical ORR polarization curves of $NF(Pt_{nano})$ composites containing Pt at levels of 5 $\mu g{\cdot}cm^{-2}$ obtained at room temperature in an O_2-saturated 0.1 M $HClO_4$ aqueous solution using a GC rotating disk electrode (RDE) at 1600 rpm, which was modified by a $NF(Pt_{nano})$ composite. The onset potential and half-wave potential positively shift in the $NF^{2nd}(Pt^{nano})$ composite, indicating that it is kinetically favorable. The high activity of the $NF^{2nd}(Pt_{nano})$ composite with a Pt loading of only 5 $\mu g{\cdot}cm^{-2}$ is

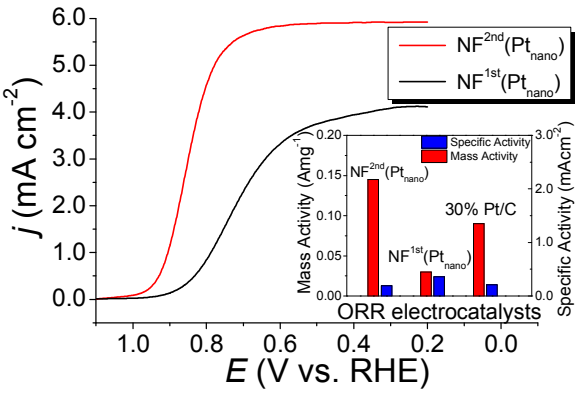

Fig. 3 ORR polarization curves of the $NF^{1st}(Pt_{nano})$ composite and $NF^{2nd}(Pt_{nano})$ composite (Pt loading: 5 μg cm^{-2})-modified GC RDE at 1600 rpm recorded in O_2-saturated 0.1 M $HClO_4$ aqueous solution. Scan rate: 0.01 $V{\cdot}s^{-1}$; temperature: 28 °C. Inset is the mass activity and specific activity (per real Pt surface area, ECSA) of $NF^{2nd}(Pt_{nano})$, $NF^{1st}(Pt_{nano})$ and 30 wt% Pt on XC-72 carbon support (Pt loading: 12.7~15.2 μg/cm^2).

demonstrated by the high onset potential of O_2 reduction (~0.95 V), and the high half-wave potential (~0.84 V), which is consistent with that of a commercial E-TEK Pt/C catalyst composed of 30 wt% Pt on the XC-72 carbon support.[1] The mass activity and specific activity (per real Pt surface area, ECSA) are good indicators of the quality of an electrocatalyst. Fig. S6a (ESI†) shows RDE polarization curves recorded for the $NF^{2nd}(Pt_{nano})$ composite (5 $\mu g{\cdot}cm^{-2}$ Pt loading)-modified GC RDE in O_2-saturated 0.1 M $HClO_4$ aqueous solution at different rotational speeds. The results strongly indicate that the four-electron ($4e^-$) reduction of O_2 is dominant for the $NF^{2nd}(Pt_{nano})$ composite, as per the Koutecký-Levich equation fitting (Fig. S6b and the experimental section in ESI†).[15] From these polarization curves, it is determined that the ORR mass activity (i_m) and ORR specific activity (i_s) at 0.9 V are 0.15 $A{\cdot}mg_{Pt}^{-1}$ and 0.20 $mA{\cdot}cm^{-2}$, respectively (Fig. 3 inset). The mass activity is higher than that of the commercial Pt/C catalyst (0.09 A mg_{Pt}^{-1}) and the $NF^{1st}(Pt_{nano})$ composite with a 40 $\mu g{\cdot}cm^{-2}$ Pt loading (0.03 $A{\cdot}mg_{Pt}^{-1}$).[1, 13] The specific activity is close to that of the commercial Pt/C catalyst (0.21 $mA{\cdot}cm^{-2}$) and $NF^{1st}(Pt_{nano})$ composite with a 40 $\mu g{\cdot}cm^{-2}$ Pt loading (0.36 $mA{\cdot}cm^{-2}$).[1]

In summary, we demonstrated the combination of the "nano-size" effect and the ability to form Cl^- complexes as being responsible for the massive electrodissolution of Pt with an ultra-high dissolution rate under acidic conditions. We also extended the massive electrodissolution of Pt to assist with the regeneration of $NF(Pt_{nano})$ composites for application to the ORR. The regeneration process modified the morphology of the NF substrate, such that its effectiveness was greatly improved because of the suitable size of its ion channels, sponge-like structure, and large surface area. The highly effective dispersion of nPts on the regenerated NF substrate significantly improved the catalytic performance of the ORR, only requiring an ultra-low Pt loading (5 $\mu g{\cdot}cm^{-2}$). Our approach can be readily extended to recycle or regenerate other noble metal-containing catalysts. In addition, the new regeneration process can successfully extend the sustainability and durability of catalyst materials and easily reproduce their performance in a wide range of applications in the fields of catalysis, energy, and sensing.

Notes and references

1. S. H. Sun, G. X. Zhang, D. S. Geng, Y. G. Chen, R. Y. Li, M. Cai and X. L. Sun, *Angew. Chem. Int. Ed.*, 2011, **50**, 422.
2. A. Morozan, B. Jousselme and S. Palacin, *Energy Environ. Sci.*, 2011, **4**, 1238.
3. Y. Bing, H. Liu, L. Zhang, D. Ghosh and J. Zhang, *Chem. Soc. Rev.*, 2010, **39**, 2184.
4. J. Zhang, K. Sasaki, E. Sutter and R. R. Adzic, *Science*, 2007, **315**, 220; Y. Nie, S. Chen, W. Ding, X. Xie, Y. Zhang and Z. Wei, *Chem. Commun.*, 2014, **50**, 15431; A. Funatsu, H. Tateishi, K. Hatakeyama, Y. Fukunaga, T. Taniguchi, M. Koinuma, H. Matsuura and Y. Matsumoto, *Chem. Commun.*, 2014, **50**, 8503.
5. H. W. Zhang and P. K. Shen, *Chem. Soc. Rev.*, 2012, **41**, 2382.
6. S. Chen, H. A. Gasteiger, K. Hayakawa, T. Tada and Y. Shao-Horn, *J. Electrochem. Soc.*, 2010, **157**, A82; P. J. Ferreira, G. J. la O, Y. Shao-Horn, D. Morgan, R. Makharia, S. Kocha and H. A. Gasteiger, *J. Electrochem. Soc.*, 2005, **152**, A2256; K. Sasaki, H. Naohara, Y. Cai, Y. M. Choi, P. Liu, M. B. Vukmirovic, J. X. Wang and R. R. Adzic, *Angew. Chem. Int. Ed.*, 2010, **49**, 8602.
7. R. Borup, J. Meyers, B. Pivovar, Y. S. Kim, R. Mukundan, N. Garland, D. Myers, M. Wilson, F. Garzon, D. Wood, P. Zelenay, K. More, K. Stroh, T. Zawodzinski, J. Boncella, J. E. McGrath, M. Inaba, K. Miyatake, M. Hori, K. Ota, Z. Ogumi, S. Miyata, A. Nishikata, Z. Siroma, Y. Uchimoto, K. Yasuda, K.-i. Kimijima and N. Iwashita, *Chem. Rev.*, 2007, **107**, 3904.
8. Y.-J. Wang, D. P. Wilkinson and J. Zhang, *Chem. Rev.*, 2011, **111**, 7625.
9. J. F. Huang and H. Y. Chen, *Angew. Chem. Int. Ed.*, 2012, **51**, 1684.
10. J.-F. Huang and M.-C. Fan, *J. Mater. Chem.*, 2010, **20**, 1431.
11. W. Lin, R.-W. Zhang, S.-S. Jang, C.-P. Wong and J.-I. Hong, *Angew. Chem. Int. Ed.*, 2010, **49**, 7929; M. A. Barakat and M. H. H. Mahmoud, *Hydrometallurgy*, 2004, **72**, 179.
12. L. Tang, B. Han, K. Persson, C. Friesen, T. He, K. Sieradzki and G. Ceder, *J. Am. Chem. Soc.*, 2010, **132**, 596.
13. J.-F. Huang and W.-R. Chang, *J. Mater. Chem.*, 2012, **22**, 17961.
14. J.-F. Huang, *J. Mater. Chem. B*, 2014, **2**, 1354; J.-F. Huang and H.-H. Chen, *Talanta*, 2013, **116**, 852.
15. A. J. Bard and L. R. Faulkner, *Electrochemical Method: Fundamentals and Applications*, 2nd ed. edn., John Wiley & Son, New York, 2001.
16. X. P. Wang, R. Kumar and D. J. Myers, *Electrochem. Solid-State Lett.*, 2006, **9**, A225.
17. H. C. Delong, J. S. Wilkes and R. T. Carlin, *J. Electrochem. Soc.*, 1994, **141**, 1000.
18. K. A. Mauritz and R. B. Moore, *Chem. Rev.*, 2004, **104**, 4535.
19. T. Xue, J. S. Trent and K. Osseoasare, *J. Membr. Sci.*, 1989, **45**, 261.